Zhang *et al.*
Chinese Journal of Mechanical Engineering (2024) 37:31
https://doi.org/10.1186/s10033-024-01007-7

Chinese Journal of Mechanical Engineering

ORIGINAL ARTICLE

Open Access

Optimization Control of Multi-Mode Coupling All-Wheel Drive System for Hybrid Vehicle

Lipeng Zhang[1*], Zijian Wang[1], Liandong Wang[1] and Changan Ren[1]

Abstract

The all-wheel drive (AWD) hybrid system is a research focus on high-performance new energy vehicles that can meet the demands of dynamic performance and passing ability. Simultaneous optimization of the power and economy of hybrid vehicles becomes an issue. A unique multi-mode coupling (MMC) AWD hybrid system is presented to realize the distributed and centralized driving of the front and rear axles to achieve vectored distribution and full utilization of the system power between the axles of vehicles. Based on the parameters of the benchmarking model of a hybrid vehicle, the best model-predictive control-based energy management strategy is proposed. First, the drive system model was built after the analysis of the MMC-AWD's drive modes. Next, three fundamental strategies were established to address power distribution adjustment and battery SOC maintenance when the SOC changed, which was followed by the design of a road driving force observer. Then, the energy consumption rate in the average time domain was processed before designing the minimum fuel consumption controller based on the equivalent fuel consumption coefficient. Finally, the advantage of the MMC-AWD was confirmed by comparison with the dynamic performance and economy of the BYD Song PLUS DMI-AWD. The findings indicate that, in comparison to the comparative hybrid system at road adhesion coefficients of 0.8 and 0.6, the MMC-AWD's capacity to accelerate increases by 5.26% and 7.92%, respectively. When the road adhesion coefficient is 0.8, 0.6, and 0.4, the maximum climbing ability increases by 14.22%, 12.88%, and 4.55%, respectively. As a result, the dynamic performance is greatly enhanced, and the fuel savings rate per 100 km of mileage reaches 12.06%, which is also very economical. The proposed control strategies for the new hybrid AWD vehicle can optimize the power and economy simultaneously.

Keywords Hybrid vehicle, All-wheel drive, Multi-mode coupling, Energy management, Model predictive control

1 Introduction

Compared to traditional fuel vehicles, new energy vehicles are more environmentally friendly and save on energy. As a result, it has become a development hotspot in recent years [1]. Among them, the hybrid vehicles have dramatically increased power output and cruising range without appreciably raising the price [2], which are now the most sought-after new energy vehicles on the market. Due to the presence of the engine, energy conservation, emissions reduction, and cost reduction are all the design goals of hybrid vehicles [3]. With the emergence of various hybrid systems, the improvement of economy and ride comfort under the presumption of ensuring power performance is the main design goal of hybrid vehicles [4]. For high-performance hybrid vehicles, the enhancement of economy is crucial for ensuring the drivability and slope pass ability [5, 6]. The conflicts between power performance and economic requirements must be resolved.

*Correspondence:
Lipeng Zhang
evzlp@ysu.edu.cn
[1] School of Vehicle and Energy, Yanshan University, Qinhuangdao 066004, China

The performance improvement channels of the hybrid vehicles are divided into energy optimization management and the configuration innovative design of the hybrid system [7]. First off, optimal power distribution and mode switching control are the simplest methods to improve system performance [8]. For a hybrid system with an automatic mechanical transmission as the mode switching control actuator, the dynamic shift schedule is used to enhance the acceleration capability of hybrid vehicles in order to improve the power performance [9]. Furthermore, selecting the most efficient gear position according to vehicle performance requirements can also further improve the fuel economy. However, because the techniques are dependent on the power source torque output, number of transmission gears, and number of driving wheels, they will be severely constrained by the drive system configuration. The performance enhancement may be accomplished in addition to the use of control and optimization algorithms by altering the structure of the transmissions [10].

From a structural standpoint, the all-wheel drive (AWD) system offers superior power performance and passing ability as compared to the two-wheel drive system [11]. Due to the rapid rise in popularity of hybrid electric vehicles, a high-performance AWD hybrid system must be developed to match driver expectations for vehicle performance. The AWD system of the four-wheel drive hybrid vehicle will output greater traction force while driving on a bumpy road or accelerating and climbing. When traveling on a level, decent road, it can be switched to two-wheel drive to save energy. So, the AWD system can meet the comprehensive requirements of power performance and economy, and is an inevitable choice for high-performance vehicles. The researchers further enhanced the AWD system's efficiency using the optimization control method. Ju et al. [12] employed a unified optimization technique to discover the best hybrid system design in the series, series-parallel, power split, and power split modes after modeling various hybrid system topologies. In this situation, the economy works best. When the optimization method has been established for the fundamental structure of a hybrid system, in order to get the optimum energy consumption performance, a second power connection device is placed between the front and rear axles, and the power split control is employed with the equivalent fuel factor [13]. A Goodarzi et al. [14] determined optimum tire force distribution in order to optimize tire usage to achieve a target vehicle response, and distributed the torque of each power source to exploit the AWD system performance. This is an alternative to the conventional power split control and predicated on enhancing the economy even more.

Although the aforementioned researches have made significant progress, there is currently no mathematical method for selecting the timing of the power source's switching, and it is not possible to transfer the axle load in either direction. To address the existence issues, the authors research team developed a brilliant multi-mode coupling AWD hybrid system named MMC-AWD with directional axle load transfer and excellent dynamic performance. The study provides a mode switching strategy that includes a formula derivation controller, a power source efficiency calculation controller, and the system itself as the research object in order to increase economy. In order to verify the superiority of the invented hybrid system, a comparative study is also carried out with the famous DMI-AWD.

This paper is organized as follows. The system configuration and drive modes of the MMC-AWD are introduced in the second chapter. The third chapter develops the vehicle model and introduces the vehicle parameters. The fourth chapter creates the vehicle control strategy and establishes the road driving force observer. The fifth chapter establishes the model predictive control (MPC) energy consumption controller based on the equivalent fuel usage, and describes the optimization results of vehicle power performance and economy obtained by using the MMC-AWD, and the comparison with the DMI-AWD is also explained. Finally, the conclusions have been reached in sixth chapter.

2 System Configuration and Working Modes of MMC-AWD

2.1 System Configuration

Figure 1 displays the mechanical characteristics of the MMC-AWD, which is a novel hybrid system that enables front-wheel drive, rear-wheel drive, or all-wheel drive from one, two or three power sources. The dual-mode coupling transmission can alternate between distributed drive mode and centralized drive mode.

When the dispersed drive mode is activated, the front motor and engine power the front axle while the rear motor powers the back axle. It is possible to implement a parallel hybrid system that combines AWD, front-wheel drive, and rear-wheel drive. When the front motor generates electricity while the rear motor drives, the series drive can be achieved. The front and rear motor, engine, can all achieve AWD by switching to the centralized drive mode. The engine and motors are operating in parallel. The power distribution of the front and rear bridges can be realized when one end of the transmission is turned into the centralized drive and the other end is switched into the distributed drive. This significantly enhances the vehicle's dynamic performance when the axles' load is transferred. Between the engine and the motor, there is

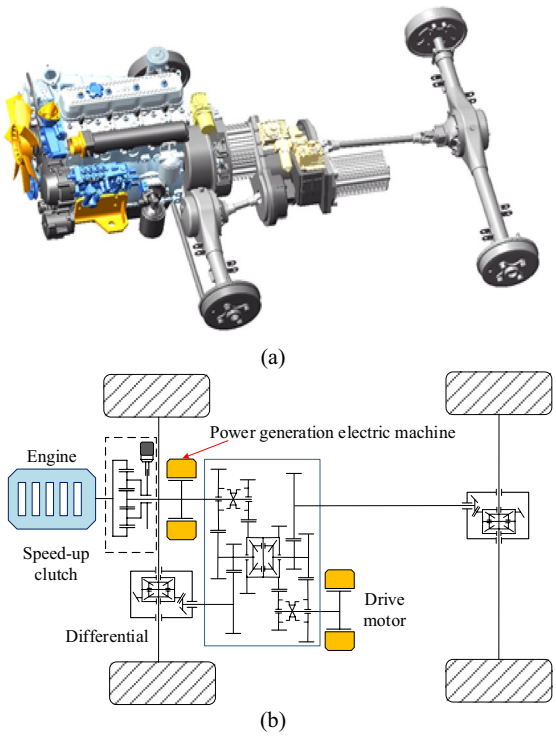

Figure 1 Configuration of MMC-AWD: (**a**) 3D structure, (**b**) Principle structure

a speed-up clutch that boosts the engine speed and syncs the high-efficiency interval with the motor.

2.2 Drive Modes Analysis

The selected drive modes, the limiting conditions for driving modes choosing, and the driving torques and electric energy transmission paths of the MMC-AWD are displayed in Table 1. According to the different driving torque requirements, the high efficient working range constraints and the residual power limits, the main drive modes include eight two-wheel drive, sixteen four-wheel drive, where the braking energy recovery is accompanied by the corresponding modes. Through the reasonable power distribution among the engine and two motors, all of the two-wheel drive modes and the four-wheel drive modes may have excellent power performance and economy. It is very important to adopt an optimal control strategy that matches the system configuration to achieve optimal energy management.

3 Hybrid System Modeling and Observer Construction

3.1 Hybrid System Modeling

3.1.1 Engine Model

The engine model's main interference, as opposed to the elements taken into account by the motor model, is its own resistance. Hence, the following equation is constructed to illustrate the connection between the driving force, resistance, and output torque. The formula is:

$$T_{\mathrm{e}} = \gamma_{\mathrm{e}} T_{\mathrm{emax}}(\omega_{\mathrm{e}}) + (1-\gamma_{\mathrm{e}}) T_{\mathrm{e\,min}}(\omega_{\mathrm{e}}), \tag{1}$$

where T_{e} is the engine output torque, $T_{\mathrm{emax}}(\omega_{\mathrm{e}})$ is the current speed corresponding to the engine maximum torque, γ_{e} is the engine throttle opening, $T_{\mathrm{emin}}(\omega_{\mathrm{e}})$ is the minimum torque (resistance moment) of the engine corresponding to the current speed, which is used to calculate the output torque after the internal resistance reduction of the engine.

3.1.2 Motor Model

A first-order inertial element serves as the motor model to represent the overshoot and hysteresis characteristics, and the formula is as follows:

$$T_{\mathrm{m}} = \begin{cases} \frac{\gamma_{\mathrm{m}}}{\tau_{\mathrm{m}} s+1} T_{\mathrm{mmax}}(\omega_{\mathrm{m}}), T_{\mathrm{m}} > 0, \\ \frac{\gamma_{\mathrm{m}}}{\tau_{\mathrm{m}} s+1} T_{\mathrm{mmin}}(\omega_{\mathrm{m}}), T_{\mathrm{m}} > 0, \end{cases} \tag{2}$$

where T_{m} is the motor output torque, $T_{\mathrm{mmax}}(\omega_{\mathrm{m}})$ is the motor maximum torque corresponding to the current speed, γ_{m} is the electromechanical throttle opening, τ_{m} is the motor response time constant, s is the time of motor response, $T_{\mathrm{mmin}}(\omega_{\mathrm{m}})$ is the motor small torque corresponding to the current speed, which is used to calculate energy recovery.

3.1.3 Battery Model

The formula for the battery model, which primarily considers the link among the SOC, voltage, current, and internal resistance, is shown below [15, 16]:

$$\mathrm{SOC_t} = \mathrm{SOC_0} - \frac{\int_{\mathrm{t_0}}^{\mathrm{t}} I_{\mathrm{L}} \mathrm{dt}}{C_{\mathrm{b}}}, \tag{3}$$

where $\mathrm{SOC_t}$ is the SOC value of the battery at t moment, $\mathrm{SOC_0}$ is the SOC value at the beginning, C_{b} is the battery capacity, I_{L} is the battery output current.

$$U_{\mathrm{b}} = U_0 - R_{\mathrm{battery}} I_{\mathrm{L}}, \tag{4}$$

Table 1 Drive modes of MMC-AWD

Drive modes	Engine distributed drives front wheels	Engine distributed drives front wheels and front motor generates electricity	Front motor distributed drives front wheels	Engine and front motor distributed drive front wheels	Front motor quickly starts engine, rear motor distributed drives front wheels	Rear motor distributed drives rear wheels and front motor generates electricity
limiting conditions	$SOC<SOC_C$, $T_{eff}<T/(ii_2\eta\eta_2)<T_{emax}$, $T<F_{xf}r$, $n_{e1}<n_e$	$SOC<SOC_C$, $T/(ii_2\eta\eta_2)<T_{eff}$, $T<F_{xf}r$, $n_{e1}<n_e$	$SOC>SOC_C$, $T<F_{xf}r$, $T_{mr}<T/(i_2\eta_2)<T_{mf}$	$SOC>SOC_C$, $T_{emax}<T/(ii_2\eta\eta_2)$, $T<F_{xf}r$, $n_{e1}<n_e$	$SOC_L<SOC<SOC_C$, $n_e>n_{e0}$, $T<F_{xf}r$, $T/(i_2\eta_2)<T_{mr}$	$SOC_L<SOC<SOC_C$, $T<F_{xf}r$, $T/(i_2\eta_2)<T_{mr}$, $T_{eff}<T_{ecmd}$
Transmission paths	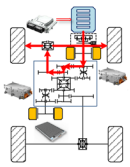	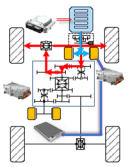	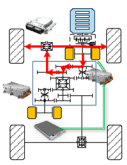	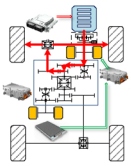	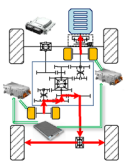	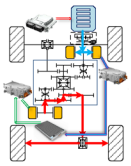
Drive modes	Rear motor distributed drives rear wheels	Two motors recover braking energy from four wheels	Front motor centralized drives four wheels	Engine centralized drives four wheels	Rear motor centralized drives four wheels and front motor generates electricity	Two motors centralized drive four wheels in parallel
limiting conditions	$SOC>SOC_C$, $T<F_{xr}r$, $T/(i_2\eta_2)<T_{mr}$	$SOC<SOC_H$, $T_b/(i_2\eta_2)<T_{mf}+T_{mr}$	$SOC>SOC_C$, $T>F_{xf}r$, $T_{mr}<T/(i_1\eta_1)<T_{mf}$	$SOC<SOC_C$, $n_{e1}<n_e$, $T>F_{xf}r$, $T_{eff}<T/(ii_1\eta\eta_1)<T_{emax}$	$SOC<SOC_C$, $T_{mcmd}i\eta=T_{mfmd}$, $T>F_{xr}r$, $T/(i_1\eta_1)<T_{mr}$	$SOC>SOC_C$, $T>F_{xr}r$, $T>F_{xf}r$, $T_{mf}<T_{mcmd}<T_{mf}+T_{mr}$
Transmission paths	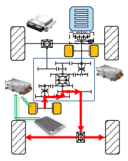	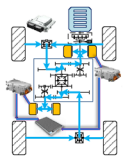	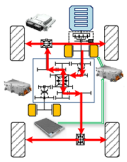	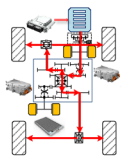	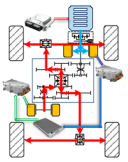	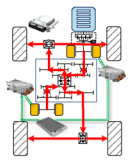
Drive modes	Rear motor centralized drives four wheels	Engine and two motors centralized drive four wheels in parallel	Two motors distributed drive four wheels	Engine distributed drives front wheels and Rear motor distributed drives rear wheels	Rear motor drives rear wheel, engine drives front wheel and front motor produces electricity	Engine and front motor drive front wheels in parallel, and rear motor drives rear wheels
limiting conditions	$SOC>SOC_C$, $T>F_{xr}r$, $T/(i_1\eta_1)<T_{mr}$	$SOC>SOC_C$, $T>F_{xr}r$, $T>F_{xf}r$, $T_{mf}+T_{mr}<T/(i_1\eta_1)<T_{mf}+T_{mr}+T_{emax}i\eta$	$SOC>SOC_C$, $T>F_{xf}r$, $T>F_{xf}r$, $T/(i_2\eta_2)<T_{mf}+T_{mr}$	$SOC>SOC_C$, $n_e>n_{e1}$ $T_{ecmd}ii_2\eta\eta_2<F_{xf}r$, $T_{mrcmd}i_2\eta_2<F_{xr}r$, $T<T_{emaxd}ii_2\eta\eta_2+T_{mr}i_2\eta_2$	$SOC<SOC_C$ $T_{ecmd}ii_2\eta\eta_2<F_{xf}r$, $T_{mrcmd}i_2\eta_2<F_{xr}r$, $T<T_{emaxd}ii_2\eta\eta_2+T_{mr}i_2\eta_2$	$SOC>SOC_C$, $(T_{ecmd}i\eta+T_{mfcmd})i_2\eta_2<F_{xf}r$, $T_{mrcmd}i_2\eta_2<F_{xr}r$, $T<(T_{emax}i\eta+T_{mf})i_2\eta_2+T_{mr}i_2\eta_2$
Transmission paths	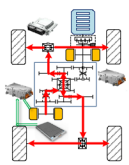	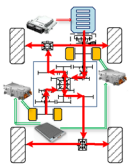	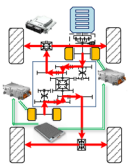	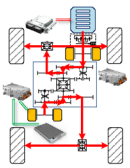	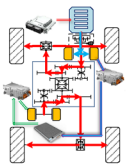	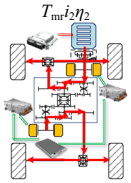
Drive modes	Front motor centralized drives four wheels and rear motor distributed drives rear wheels	Rear motor centralized drives four wheels and front motor distributed drives front wheels	Engine centralized drives four wheels and rear motor distributed drives rear wheels	Engine distributed drives front wheels and rear motor centralized drives four wheels	Rear motor drives four wheels, engine drives front wheels and front motor produces electricity	Engine and front motor centralized drive four wheels, rear motor distributed drives rear wheels
limiting conditions	$SOC>SOC_C$, $F_{xf}<F_{xr}$, $T_{mf}i_1\eta_1<T<T_{mf}i_1\eta_1+T_{mr}i_2\eta_2$	$SOC>SOC_C$, $F_{xf}>F_{xr}$, $T_{mr}i_1\eta_1<T<T_{mf}i_2\eta_2T_{mr}i_1\eta_1$	$SOC>SOC_C$, $F_{xf}<F_{xr}$, $n_{e1}<n_e$, T_{eff} $ii_1\eta\eta_1+T_{mr}i_2\eta_2<T<T_{emax}ii_1\eta\eta_1+T_{mr}i_2\eta_2$	$SOC<SOC_C$, $F_{xf}>F_{xr}$, $n_{e1}<n_e$, $T_{ecmd}>T_{eff}$, $T_{ecmd}i\eta>T_{mfcmd}$, $T_{mr}i_1\eta_1<T<(T_{emax}i\eta-T_{mfcmd})i_2\eta_2+T_{mr}i_1\eta_1$	$SOC>SOC_C$, $F_{xf}<F_{xr}$, $n_{e1}<n_e$, $T_{eff}ii_2\eta\eta_2+T_{mr}i_1\eta_1<T<(T_{emax}i\eta+T_{mf})i_2\eta_2+T_{mr}i_1\eta_1$	$SOC>SOC_C$, $F_{xf}<F_{xr}$, $n_{e1}<n_e$, $T_{eff}ii_1\eta\eta_1+T_{mr}i_2\eta_2<T<(T_{emax}i\eta+T_{mf})i_1\eta_1+T_{mr}i_2\eta_2$
Transmission paths	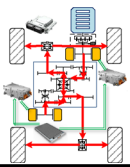	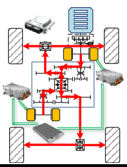	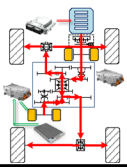	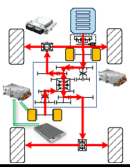	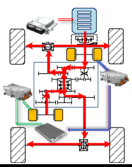	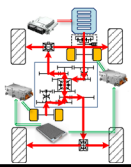

where U_b is the battery terminal voltage, U_0 is the battery open circuit voltage, and $R_{battery}$ is the battery internal resistance.

$$I_L=\frac{U_0-\sqrt{U_0-4R_{battery}P_m}}{2R_{battery}}, \tag{5}$$

where P_m is the motor power.

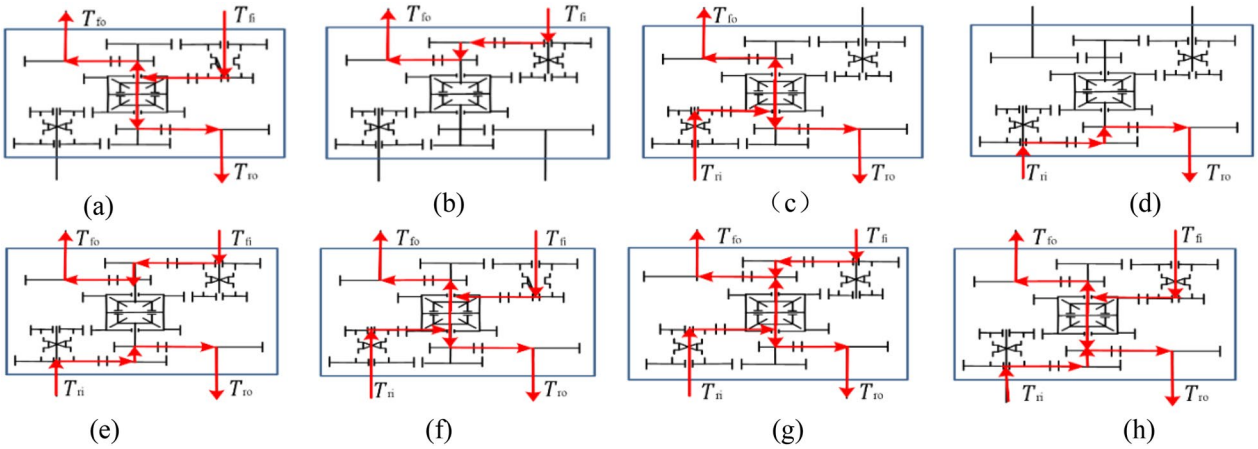

Figure 2 Different drive modes of dual-mode coupling transmission: (**a**) Front input and four-wheel centralized drive, (**b**) Front input and front axle distributed drive, (**c**) Rear input and four-wheel centralized drive, (**d**) Rear input and rear axle distributed drive, (**e**) Front and rear axles distributed drive, (**f**) Front and rear axles centralized drive, (**g**) Front axle distributed drive and rear axle centralized drive, (**h**) Rear axle distributed drive and front axle centralized drive

3.1.4 Speed-Up Clutch Model

According to the difference between the sliding and engagement states, the torques transmitted by the speed-up clutch are [17]:

$$T_c = \begin{cases} \mu_c A_c P_c \mathrm{sgn}(\omega_1 - \omega_2) i\eta, & \text{slidingstate}, \\ T_e i\eta, & \text{engagementstate}, \end{cases} \tag{6}$$

where T_c is the clutch transmission torque, μ_c is the dynamic friction coefficient between the friction surfaces, P_c is the contact surface pressure, A_c is the effective contact area, ω_1 is the input speed, ω_2 is the output speed.

3.1.5 Transmission Model

Different modes of the centralized, distributed and coupling drive can be realized through the modes switching of dual-mode coupling transmission, as shown in Figure 2, where T_{fi} represents the drive torque input from the front side, T_{ri} represents the drive torque input from the rear side, T_{fo} represents the torque output from the front axle, and T_{ro} represents the torque output from the rear axle. In this figure, the torque transmission paths are also represented.

According to different drive modes, the driving torque output from the front and rear axles can be expressed as:

$$T_{fo} = \begin{cases} T_{fi} i_2 \eta_2, \\ T_{fi} i_1 \eta_1 / 2, \\ 0, \\ T_{ri} i_1 \eta_1 / 2, \\ T_{ri} i_2 \eta_2, \\ (T_{fi} + T_{ri}) i_1 \eta_1 / 2, \\ T_{ri} i_1 \eta_1 / 2 + T_{fi} i_2 \eta_2, \\ T_{fi} i_2 \eta_2 / 2, \end{cases} \tag{7}$$

$$T_{ro} = \begin{cases} 0, \\ T_{fi} i_1 \eta_1 / 2, \\ T_{ri} i_2 \eta_2, \\ T_{ri} i_1 \eta_1 / 2, \\ T_{ri} i_2 \eta_2, \\ (T_{fi} + T_{ri}) i_1 \eta_1 / 2, \\ T_{ri} i_1 \eta_1 / 2, \\ T_{fi} i_1 \eta_1 / 2 + T_{ri} i_2 \eta_2. \end{cases} \tag{8}$$

3.2 Observer Construction

The vehicle longitudinal dynamics model is [18]:

$$F = \Delta m a + \frac{C_D A_D V^2}{21.15} + Gf + Gi_R, \tag{9}$$

where F is the wheel driving force, Δ is the rotational mass conversion coefficient, m is the full load mass, C_D is the air resistance coefficient, V is the speed of vehicle, G is the gravity, f is the road resistance coefficient, A_D is the windward area, and i_R is the slope.

The formulation can be simplified as:

$$a = \frac{F}{\Delta m} - \frac{C_D A_D V^2}{21.15 \Delta m} - \frac{Gf}{\Delta m} - \frac{Gi_R}{\Delta m}. \tag{10}$$

The following first-order nonlinear system is provided:

$$\ddot{x} = f(\dot{x}) + bu. \tag{11}$$

Substitute Eq. (11) into Eq. (12) to obtain:

$$\ddot{x} = \frac{1}{\Delta m} u - f(\dot{x}) - A_1. \tag{12}$$

Given a virtual control quantity, the virtual control quantity is used to linearize the nonlinear system, then Eq. (12) can be written as:

$$u_g = \Delta m(u_0 + \frac{C_D A_D V^2}{21.15\Delta m} + A_1), \tag{13}$$

where u_g is the control quantity, A_1 is the constant formula without the state quantity.

The virtual control function is constructed as follows:

$$u_0(t) = k_1(\dot{x}_{order} - \dot{x}(t)) + k_2(\ddot{x}_{order}(t)/k_3), \tag{14}$$

where k_1 and k_2 are the virtual state quantity coefficients, k_3 is the proportional coefficient of k_1 and k_2, and $u_0(t)$ is the virtual control quantity of change.

According to the Laplace transform, convergence occurs when k_1 and k_2 are both less than 0.

Substitute Eq. (14) into Eq. (13) to obtain the observer output u_g, then the wheel driving torque is:

$$T_r(t) = u_g(t)\Delta m r, \tag{15}$$

where $T_r(t)$ is the wheel driving torque that changes with time, r is the wheel radius, and $u_g(t)$ is the actual control quantity that changes.

4 Controller Design

4.1 Control Strategy Formulation

An effective and well-organized control approach is highly beneficial for lowering the energy consumption of the hybrid vehicle after the road demand torque observation is finished. Hybrid systems based on transmission for power coupling typically have similar control architectures. The transmission ratio, driver input, vehicle speed, SOC, road driving force, motor and engine driving force, and energy consumption traits are some of the input variables. The output consists of the commands for the motor and engine's torque, the clutch, power generation, engine ignition, generator start, MPC controller activation, braking command, etc. [19, 20].

The battery's SOC, which can be divided into three categories, dictates the overall approach. However, regardless of the approach, the engine will start at idle speed. During the startup, the motor will aid the vehicle, which will cause it to move from a standstill position while also revving the engine. When the battery SOC is sufficient to support the electric propulsion for an extended period of time, the first method is enabled not requiring engine charging. It can be broken down into three fundamental modes: Engine starts with high efficient, single power source drives with MPC controller, and hybrid drive. Most of the time, the vehicle will run in the first strategy's second basic mode. The second or third technique is used when the battery's SOC reaches a specified level.

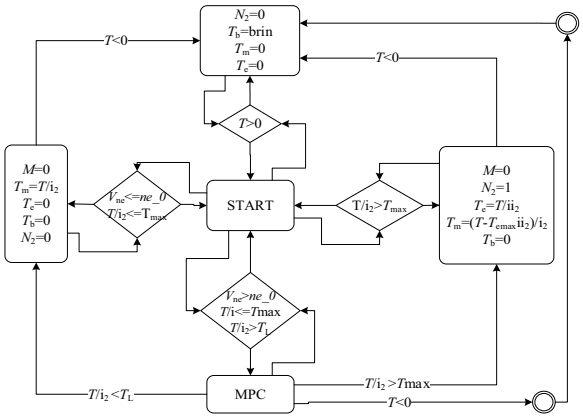

Figure 3 The first control strategy

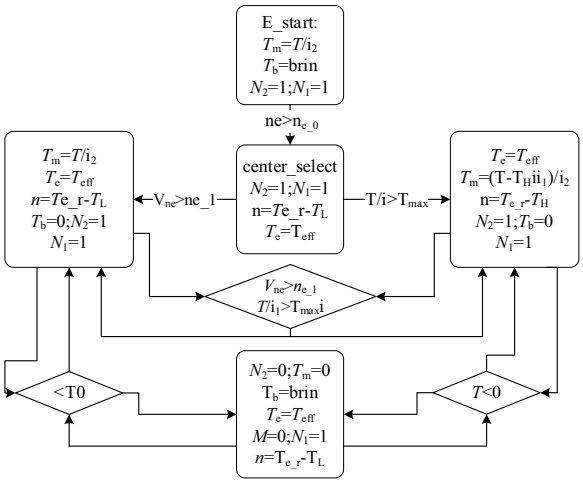

Figure 4 The second control strategy

The framework of the first tactic of the MMC-AWD is depicted as shown in Figure 3.

When the battery has a low SOC but can still sustain an effective pure electric drive, the second strategy can be used. In addition to the starting module, the second strategy can be separated into series drive mode and parallel drive mode. Although a parallel drive generates less power, it has a high-power performance. The illustration below depicts the precise architecture of the second control strategy of the MMC-AWD as shown in Figure 4.

Setting a lower limit for battery SOC is the third tactic. The battery may still discharge electric energy, but because of its high internal resistance and low driving efficiency, it is not efficient. Only the engine is used to propel the vehicle, and a generator is used to periodically recharge the battery. In addition to the high-efficiency starting module, the third approach is divided into two modes based on the change in road driving force. The

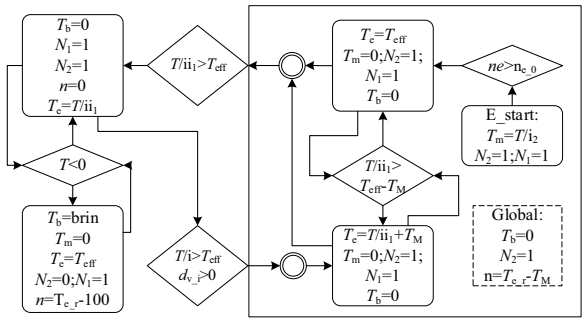

Figure 5 The third control strategy

engine only provides propulsion, or propulsion and power generation. There are two types of power generation: effective and emergency power generation. Figure 5 depicts the precise framework for the third strategy for the MMC-AWD.

4.2 MPC Controller Design

The following formula is used to calculate the equivalent fuel consumption coefficient [21–23]:

$$\lambda_{\mathrm{equ}}(t)=\frac{1}{\eta_{\mathrm{emax}}\eta_{\mathrm{m}}(t)\eta_{\mathrm{char}}}, \tag{16}$$

where $\lambda_{\mathrm{equ}}(t)$ is the time-varying equivalent fuel consumption coefficient, $\eta_{\mathrm{m}}(t)$ is the time-varying motor efficiency, η_{emax} is the maximum engine efficiency, and η_{char} is the average battery charging efficiency.

The calculation formula of the fuel calorific value is [24–26]:

$$R_{\mathrm{lhv}}=\frac{R_{\mathrm{ori}}\rho}{1000}, \tag{17}$$

where R_{lhv} is the fuel calorific value constant used for energy consumption calculation, R_{ori} is the standard fuel calorific value, ρ is the fuel density.

The equivalent fuel consumption of the motor is:

$$Q_m(t)=\lambda_{\mathrm{equ}}(t)\frac{P_{\mathrm{m}}(t)}{\eta_{\mathrm{dis}}R_{\mathrm{lhv}}}, \tag{18}$$

where η_{dis} is the average discharge efficiency of the battery, $P_{\mathrm{m}}(t)$ is the time-varying instantaneous power of the motor, and $Q_{\mathrm{m}}(t)$ is the time-varying instantaneous equivalent fuel consumption of the motor.

The fuel consumption of the engine is:

$$Q_{\mathrm{e}}(t)=\frac{p_{\mathrm{e}}(t)b_{\mathrm{e}}(t)}{367.1\rho g}, \tag{19}$$

where $P_{\mathrm{e}}(t)$ is the time-varying engine power, $b_{\mathrm{e}}(t)$ is the time-varying fuel consumption, $Q_{\mathrm{e}}(t)$ is the time-varying instantaneous engine fuel consumption, and g is the gravity acceleration.

The general form of the discrete equation of the state is [27–30]:

$$\boldsymbol{Z}_{(k+1)}=\boldsymbol{A}\boldsymbol{Z}_{(k)}+\boldsymbol{B}u_{\mathrm{z}}, \tag{20}$$

where $\boldsymbol{Z}$ is the state quantity, $\boldsymbol{A}$ is the state transition matrix, $\boldsymbol{B}$ is the control quantity matrix, u_{z} is the control quantity.

The following equation of the state can be created by substituting Eqs. (16), (17), (18), and (19) into Eq. (20), using fuel consumption as the state quantity and the instantaneous ratio of engine power to total power as the control quantity:

$$\begin{aligned}\boldsymbol{W}_{(k+1)}=&\begin{bmatrix}1&0\\0&1\end{bmatrix}\boldsymbol{W}_{(k)}\\&+\begin{bmatrix}0&\frac{p_{\mathrm{e}}(t)b_{\mathrm{e}}(t)}{367.1\rho g}\\\lambda_{\mathrm{equ}}(t)\frac{P_{\mathrm{m}}(t)}{\eta_{\mathrm{dis}}R_{\mathrm{lhv}}}&-\lambda_{\mathrm{equ}}(t)\frac{P_{\mathrm{m}}(t)}{\eta_{\mathrm{dis}}R_{\mathrm{lhv}}}\end{bmatrix}\begin{bmatrix}1\\\lambda\end{bmatrix},\end{aligned} \tag{21}$$

where $\boldsymbol{W}(k)$ is the cumulative fuel consumption at time k, $\boldsymbol{W}(k+1)$ is the cumulative fuel consumption at time $k+1$, and λ is the control quantity, which can be simplified into the general form:

$$\begin{aligned}\boldsymbol{W}_{(k+1)}=&\begin{bmatrix}1&0\\0&1\end{bmatrix}\boldsymbol{W}_{(k)}+\begin{bmatrix}\frac{p_{\mathrm{e}}(t)b_{\mathrm{e}}(t)}{367.1\rho g}\\-\lambda_{\mathrm{equ}}(t)\frac{P_{\mathrm{m}}(t)}{\eta_{\mathrm{dis}}R_{\mathrm{lhv}}}\end{bmatrix}\lambda\\&+\begin{bmatrix}0\\\lambda_{\mathrm{equ}}(t)\frac{P_{\mathrm{m}}(t)}{\eta_{\mathrm{dis}}R_{\mathrm{lhv}}}\end{bmatrix}.\end{aligned} \tag{22}$$

To summarize the control quantity in the time domain, some variables are assumed:

$$\boldsymbol{A}=\begin{bmatrix}1&0\\0&1\end{bmatrix},\quad \boldsymbol{B}=\begin{bmatrix}\frac{p_{\mathrm{e}}(t)b_{\mathrm{e}}(t)}{367.1\rho g}\\-\lambda_{\mathrm{equ}}(t)\frac{P_{\mathrm{m}}(t)}{\eta_{\mathrm{dis}}R_{\mathrm{lhv}}}\end{bmatrix},$$

$$\boldsymbol{C}=\begin{bmatrix}0\\\lambda_{\mathrm{equ}}(t)\frac{P_{\mathrm{m}}(t)}{\eta_{\mathrm{dis}}R_{\mathrm{lhv}}}\end{bmatrix},u_z=\lambda,\boldsymbol{W}_{(k)}=\begin{bmatrix}W_{\mathrm{e}}\\W_{\mathrm{m}}\end{bmatrix}.$$

After simplifying the above formula, the n term is:

$$\begin{aligned}\boldsymbol{W}_{(k+n)}=&\boldsymbol{A}^n\boldsymbol{W}_{(k)}+\boldsymbol{A}^{n-1}\boldsymbol{B}u_{(k)}\\&+\ldots+\boldsymbol{A}^{n-1}\boldsymbol{B}u_{(k+n)}+\boldsymbol{C}+\ldots+\boldsymbol{A}^{n-1}\boldsymbol{C}.\end{aligned} \tag{23}$$

The MPC prediction time domain is now set to n, and a matrix representation of the total fuel consumption in the prediction time domain is given:

$$X_k = \begin{bmatrix} W_{(k+1|k)} \\ W_{(k+2|k)} \\ W_{(k+3|k)} \\ \cdot \\ \cdot \\ W_{(k+n|k)} \end{bmatrix} = \begin{bmatrix} \boldsymbol{I} & & & & & \\ \boldsymbol{A} & \boldsymbol{I} & & & & \\ \boldsymbol{A}^2 & \boldsymbol{A} & \boldsymbol{I} & & & \\ \cdot & \cdot & \cdot & \cdot & & \\ \cdot & \cdot & \cdot & \cdot & \cdot & \\ \boldsymbol{A}^{n-1} & \boldsymbol{A}^{n-2} & \cdot & \cdot & \boldsymbol{A} & \boldsymbol{I} \end{bmatrix} \begin{bmatrix} \boldsymbol{C} \\ \boldsymbol{C} \\ \boldsymbol{C} \\ \cdot \\ \cdot \\ \boldsymbol{C} \end{bmatrix}$$
$$+ \begin{bmatrix} \boldsymbol{A}^1 \\ \boldsymbol{A}^2 \\ \boldsymbol{A}^3 \\ \cdot \\ \cdot \\ \boldsymbol{A}^n \end{bmatrix} W_{(k|k)} + \begin{bmatrix} \boldsymbol{B} & & & & & \\ \boldsymbol{A}^2\boldsymbol{B} & \boldsymbol{B} & & & & \\ \boldsymbol{A}^3\boldsymbol{B} & \boldsymbol{A}^2\boldsymbol{B} & \boldsymbol{B} & & & \\ \cdot & \cdot & \cdot & \cdot & & \\ \cdot & \cdot & \cdot & \cdot & \cdot & \\ \boldsymbol{A}^n\boldsymbol{B} & \boldsymbol{A}^{n-1}\boldsymbol{B} & \cdot & \cdot & \boldsymbol{A}^2\boldsymbol{B} & \boldsymbol{B} \end{bmatrix} \begin{bmatrix} u_{(k+1|k)} \\ u_{(k+2|k)} \\ u_{(k+3|k)} \\ \cdot \\ \cdot \\ u_{(k+n|k)} \end{bmatrix}. \tag{24}$$

Type of $\boldsymbol{W}_{(k+i|\,k)}$ is the first time predicted by the first $k+i$ moment instantaneous fuel consumption, the overall fuel consumption in the time domain can be predicted by $X_{(k)}$. Some variables are assumed as:

$$\boldsymbol{L} = \begin{bmatrix} \boldsymbol{A}^1 \\ \boldsymbol{A}^2 \\ \boldsymbol{A}^3 \\ \cdot \\ \cdot \\ \boldsymbol{A}^n \end{bmatrix}, \bar{\boldsymbol{C}} = \begin{bmatrix} \boldsymbol{C} \\ \boldsymbol{C} \\ \boldsymbol{C} \\ \cdot \\ \cdot \\ \boldsymbol{C} \end{bmatrix}, \boldsymbol{N} = \begin{bmatrix} \boldsymbol{I} & & & & & \\ \boldsymbol{A} & \boldsymbol{I} & & & & \\ \boldsymbol{A}^2 & \boldsymbol{A} & \boldsymbol{I} & & & \\ \cdot & \cdot & \cdot & \cdot & & \\ \cdot & \cdot & \cdot & \cdot & \cdot & \\ \boldsymbol{A}^{n-1} & \boldsymbol{A}^{n-2} & \cdot & \cdot & \boldsymbol{A} & \boldsymbol{I} \end{bmatrix}$$
$$, \boldsymbol{Y} = \begin{bmatrix} \boldsymbol{B} & & & & & \\ \boldsymbol{A}^2\boldsymbol{B} & \boldsymbol{B} & & & & \\ \boldsymbol{A}^3\boldsymbol{B} & \boldsymbol{A}^2\boldsymbol{B} & \boldsymbol{B} & & & \\ \cdot & \cdot & \cdot & \cdot & & \\ \cdot & \cdot & \cdot & \cdot & \cdot & \\ \boldsymbol{A}^n\boldsymbol{B} & \boldsymbol{A}^{n-1}\boldsymbol{B} & \cdot & \cdot & \boldsymbol{A}^2\boldsymbol{B} & \boldsymbol{B} \end{bmatrix}, \boldsymbol{U}_k = \begin{bmatrix} u_{(k+1|k)} \\ u_{(k+2|k)} \\ u_{(k+3|k)} \\ \cdot \\ \cdot \\ u_{(k+n|k)} \end{bmatrix}.$$

In standard form:

$$\boldsymbol{X}_k = \boldsymbol{L}\boldsymbol{W}_k + \boldsymbol{Y}\boldsymbol{U}_k + \boldsymbol{N}\bar{\boldsymbol{C}}. \tag{25}$$

The cost function can generally be written as follows:

$$\boldsymbol{J} = (\boldsymbol{X}_k - \boldsymbol{R}_k)^{\mathrm{T}}\boldsymbol{Q}(\boldsymbol{X}_k - \boldsymbol{R}_k) + \boldsymbol{U}_k^{\mathrm{T}}\boldsymbol{R}\boldsymbol{U}_k, \tag{26}$$

where $\boldsymbol{J}$ is the cost function, $\boldsymbol{X}_k$ is the state quantity, $\boldsymbol{R}_k$ is the target quantity, $\boldsymbol{Q}$ is the weight matrix of the state quantity, and R is the weight matrix of the control quantity. The control objective is to switch the power source, which is discrete and allows the control quantity to jump greatly. R is set as 0 matrix. Substitute Eq. (25) into Eq. (26), and the following equation can be obtained:

$$\begin{aligned} \boldsymbol{J} = {} & \boldsymbol{U}_k^{\mathrm{T}}\boldsymbol{Y}^{\mathrm{T}}\boldsymbol{Q}\boldsymbol{Y}\boldsymbol{U}_k + (2(\boldsymbol{N}\bar{\boldsymbol{C}} + \boldsymbol{X}_k\boldsymbol{L})^{\mathrm{T}}\boldsymbol{Q}\boldsymbol{Y})^{\mathrm{T}}\boldsymbol{U}_k \\ & + (\boldsymbol{N}\bar{\boldsymbol{C}} + \boldsymbol{X}_k\boldsymbol{L})^{\mathrm{T}}\boldsymbol{Q}(\boldsymbol{N}\bar{\boldsymbol{C}} + \boldsymbol{X}_k\boldsymbol{L}). \end{aligned} \tag{27}$$

In Eq. (24), the variable element multiplied by $\boldsymbol{Q}$ matrix in the third term has been included by the second term, which has little influence on the controller. Moreover, it has the dimension problem, which cannot be combined with the first term, so it is ignored. Then, quadratic programming equations can be established to find the optimal solution at every moment. The cost function equations are established as follows:

$$\begin{cases} \boldsymbol{H} = 2\boldsymbol{Y}^{\mathrm{T}}\boldsymbol{Q}\boldsymbol{Y}, \\ \boldsymbol{f}^{\mathrm{T}} = (2(\boldsymbol{N}\bar{\boldsymbol{C}} + \boldsymbol{X}_k\boldsymbol{L})^{\mathrm{T}}\boldsymbol{Q}\boldsymbol{Y})^{\mathrm{T}}, \\ \boldsymbol{J} = \boldsymbol{U}_k^{\mathrm{T}}\boldsymbol{H}\boldsymbol{U}_k + \boldsymbol{f}^{\mathrm{T}}\boldsymbol{U}_k. \end{cases} \tag{28}$$

The future control quantity U_{n} calculated at this time is ignored after the optimal control quantity group $\boldsymbol{U}_{\mathrm{k}}$ is obtained by MATLAB/Simulink, and the first item U_1, which is an arbitrary decimal between [0, 1], is taken as the current control quantity. Then the MPC fuel calculation for the hybrid drive ratio can be obtained. When the torque does not reach the maximum value of a single power source, the efficiency of the single power source is higher, so the torque sharing between the engine and motor is started at different times in order to make the motor and engine work in the high torque region and improve overall economy. The oil power distribution can now be calculated with Eq. (29), which will result in the best single power source choice.

$$k_{\mathrm{c}} = \frac{1 + \mathrm{sgn}((\sum_1^{\mathrm{h}} u_{\mathrm{i}})/k_{\mathrm{h}} - 0.5)}{2}, \tag{29}$$

where k_{c} is the power source selection coefficient, h is the h moment, U_{i} is the i-control quantity, k_{h} is the number of moments. Taking the average value of a control quantity as switching condition can avoid the energy loss caused by frequent switching of power source.

According to the above analysis, the total vehicle power has the following relationship with motor and engine power:

$$P = k_{\mathrm{c}}P_{\mathrm{e}} + (1 - k_{\mathrm{c}})P_{\mathrm{m}}, \tag{30}$$

where P_{e} is the engine power and P_{m} is the motor power.

As the use time of the vehicle increases, the battery internal resistance rises and the capacity decreases. The temperature of the battery will increase along with the internal resistance when the vehicle is experiencing rapid acceleration, climbing or other high load conditions. The vehicle efficiency is not impacted by capacity because the control policy does not utilize the peak capacity. Additionally, each SOC switching threshold of the strategies can increases or decreases within a reasonable and small range using the idea of "equivalent fuel consumption", electricity and fuel are calculated in unison, and the conversion to each other does not change the economy. However, variations in battery internal resistance will impact the battery efficiency and alter the control scheme. The details of the energy flows are shown in Figure 6. The following equation describes how to handle variations in battery-resistance.

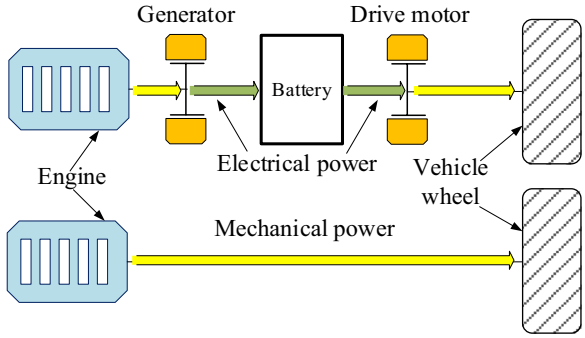

Figure 6 Diagram of different energy flows

Calculating the engine's energy consumption and comparing it to the motor's usage allows the MPC control logic to switch power sources. The energy can be divided into two categories: (1) Engine - generator - battery - motor – wheel; (2) engine – wheel. The most efficient mode can be calculated by the MPC. Before this, we need to prepare the equivalent fuel consumption factor to convert the power consumption into fuel consumption, which is part of the controller.

The calculation formula for the equivalent fuel consumption coefficient of battery efficiency change is:

$$\lambda_{\mathrm{equ}}(t)=\frac{1}{\eta_{\mathrm{emax}}\eta_{\mathrm{m}}(t)\eta_{\mathrm{char}}(t)}. \tag{31}$$

In a similar way, equivalent fuel consumption of the motor is:

$$Q_{\mathrm{m}}(t)=\lambda_{\mathrm{equ}}(t)\frac{P_{\mathrm{m}}(t)}{\eta_{\mathrm{dis}}(t)R_{\mathrm{lhv}}}. \tag{32}$$

It follows that a change in battery resistance can be replaced by a change in efficiency in the control strategy. Because calculating battery efficiency from unknown internal resistance and changing terminal voltage is difficult, the following methods are used to calculate battery charge and discharge efficiency:

$$\eta_{\mathrm{char}}(t)=\frac{U_{\mathrm{g}}(t)I_{\mathrm{g}}(t)\Delta t}{3.6\times10^{7}W\Delta\mathrm{SOC}}, \tag{33}$$

where $U_{\mathrm{g}}(t)$ is the generator terminal voltage, $I_{\mathrm{g}}(t)$ is the generator electric current, Δt is a period of time, and W is the battery electrical energy in kW·h. ΔSOC is the battery SOC change value. The efficiency of the battery charge is represented by $\eta_{\mathrm{char}}(t)$.

$$\eta_{\mathrm{dis}}(t)=\frac{3.6\times10^{7}W\Delta\mathrm{SOC}}{U_{\mathrm{m}}(t)I_{\mathrm{m}}(t)\Delta t}, \tag{34}$$

where $\eta_{\mathrm{dis}}(t)$ represents the efficiency of the battery discharge, $U_{\mathrm{m}}(t)$ is the drive motor voltage, $I_{\mathrm{m}}(t)$ is the drive motor electric current.

The cell efficiency for any time period can be calculated using the aforementioned two formulas. Additionally, it can be incorporated into the MPC controller, and the control strategy changed using the "equivalent fuel consumption coefficient" in Eq. (32). The dynamic efficiency of the cell can be calculated.

4.3 Control System Architecture

Figure 7 displays the architecture and vehicle control system. The brown dotted box represents the nonlinear observer, the blue dotted box represents the state flow control scheme, the green dotted box represents the MPC energy consumption controller, and the green solid box represents the vehicle model. MPC energy consumption controller output engine clutch contact instruction, engine torque and motor torque. The output of the controller affects the entire vehicle and is combined with the output value of the vehicle strategy.

5 Comparison Analysis and Simulation Verifiction

5.1 Comparison and Simulation Conditions

To verify the superiority of the power performance and economy of the invented MMC-AWD, the DMI-AWD is used for comparison. The selected drive modes, the limiting conditions for driving mode optimization, and the driving torque and electric energy transmission paths of the DMI-AWD are displayed in Table 2, where i_{d} is the transmission ratio from engine to front wheel, η_{d} is the transmission efficient from engine to front wheel, i_{f} is the transmission ratio from engine to front wheel, η_{f} is the transmission efficient from front motor to front wheel, i_{r} is the transmission ratio from front motor to front wheel, η_{r} is the transmission efficient from the rear motor to the rear wheel. These modes are discovered by an examination of the motor, engine, and transmission characteristics.

There are three modes of four-wheel drive and power generation, as well as five modes of two-wheel drive and brake energy recovery.

Both the MMC-AWD and DMI-AWD are employed two-wheel drive modes in the economic comparison and four-wheel drive modes in the power performance comparison. The power performance can be analyzed using the maximum climb and 100 km/h acceleration, but these two metrics will vary depending on the state of the road. The 100 km/h acceleration and maximum climb will be impacted by the low road adhesion coefficient. It has become crucial to figure out how to lessen the impact they have. When the axle load is transferred backwards during acceleration and hill climbing conditions, the

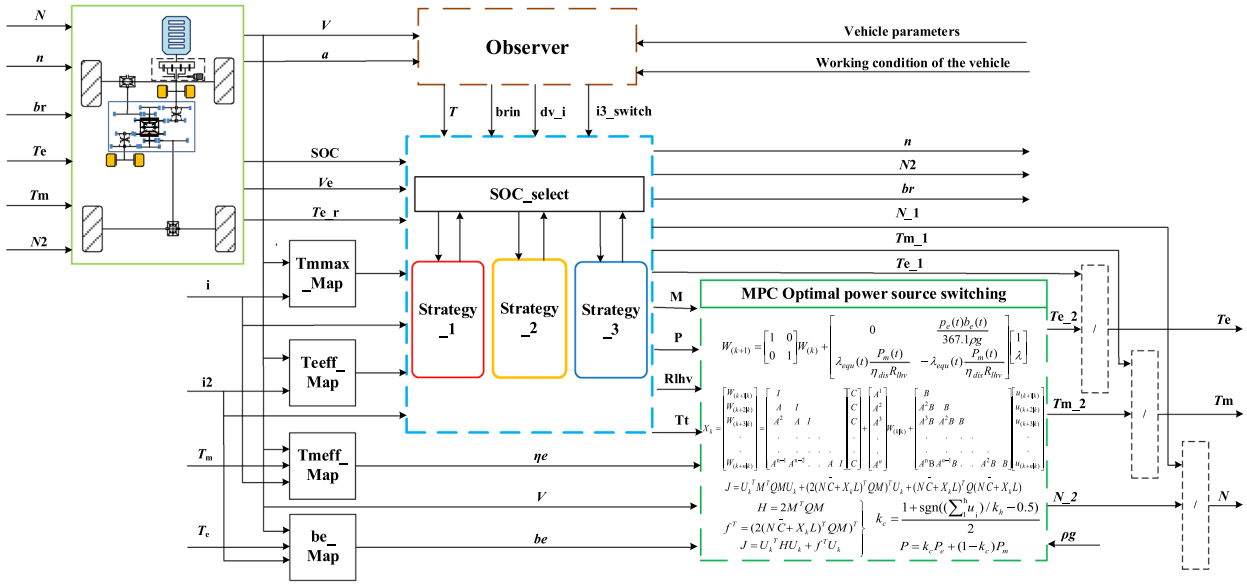

Figure 7 Control system architecture

Table 2 Drive modes of DMI-AWD

Drive modes	Engine and front motor drive front wheel, generator generates electricity	Front motor drives front wheels	Rear motor drives rear wheels	Two motors recover braking energy
Limiting conditions	$SOC < SOC_C$, $n_{e1} < n_e$, $T < F_{xf}r$, $T_{eff}i_d\eta_d < T < T_{emax}i_d\eta_d + T_{mf}i_f\eta_f$	$SOC > SOC_C$, $T < F_{xf}r$, $T_{mr}i_r\eta_r < T < T_{mf}i_f\eta_f$	$SOC > SOC_C$, $T < F_{xr}r$, $T < T_{mr}i_r\eta_r$	$SOC < SOC_H$, $T_b < T_{mf}i_f\eta_f + T_{mr}i_r\eta_r$
Transmission paths	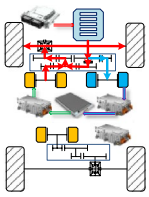	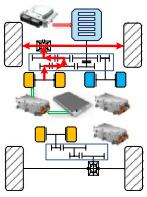	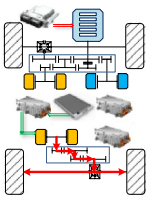	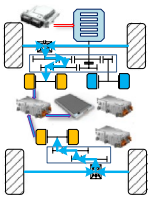
Drive modes	Engine generates electricity, front motor drives front wheels	Engine generates electricity, rear motor drives rear wheels	Front motor drives front wheels, rear motor drives rear wheels	Engine and front motor drive front wheels, rear motor drives rear wheels
Limiting conditions	$SOC_C > SOC > SOC_L$, $T < F_{xf}r$, $T < T_{mf}i_f\eta_f$	$SOC_C > SOC > SOC_L$, $T < F_{xf}r$, $T < T_{mr}i_r\eta_r$	$SOC > SOC_C$, $T > F_{xr}r$, $T > F_{xf}r$, $T < T_{mf}i_f\eta_f + T_{mr}i_r\eta_r$	$SOC > SOC_C$, $n_{e1} < n_e$, $T > F_{xr}r$, $T > F_{xf}r$, $T_{mf}i_f\eta_f + T_{mr}i_r\eta_r < T < T_{emax}i_d\eta_d + T_{mf}i_f\eta_f + T_{mr}i_r\eta_r$
Transmission paths	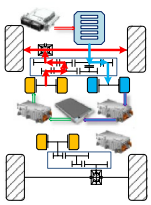	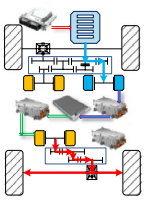	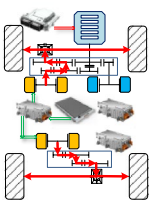	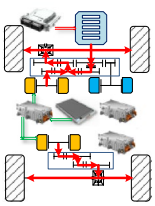

coupling drive system can transfer power from the front axle to the rear axle, allowing the vehicle's power performance to be fully unleashed.

5.2 Vehicle Parameters and System Efficiency

The vehicle parameters are shown in Table 3. The DMI-AWD has two drive motors and one generator. The MMC-AWD has only two motors, and the front motor

Table 3 Vehicle parameters

Type	The parameter name	Value
vehicle	Curb mass (kg)	1815
	Vehicle frontal area (m^2)	2.6
	Rolling resistance coefficient	0.01
	Wheel radius (m)	0.358
	Rotary mass conversion coefficient	1.05
	Coefficient of air resistance	0.35
engine	Rated torque (N·m)	231
	Rated power (kW)	102
	Highest speed (r/min)	6000
Front motor	Highest speed (r/min)	16000
	Peak torque (T)	316
	Peak power (kW)	145
Rear motor	Highest speeds (r/min)	16000
	Peak torque (T)	280
	Peak power (kW)	120
Generator of DMI	Highest speeds (r/min)	16000
	Peak torque (T)	196
	Peak power (kW)	90
Battery	Rated voltage (V)	521
	Battery capacity (kW·h)	18.3
	SOC upper limit (%)	95
	SOC lower limit (%)	5
Transmission of MMC	First gear reduction ratio (centralized)	1.2
	Second gear reduction ratio (distributed)	0.8
Reducer	Main reduction ratio	3
	Motor end speed ratio	3
	Engine end speed ratio	1.25
Transmission efficiency	One pair of gears for reduction	0.98
	Two pairs of gears decelerator	0.9604
	Differential	0.98

can generate electricity. The DMI-AWD has two fixed ratio reducer, while the MMC-AWD has a two-speed transmission. In the distributed drive mode of the MMC-AWD, the final speed ratio of the motor and engine is the same as the front wheels drive system of the DMI-AWD. Figures 8, 9, 10, 11, 12 display the operation and efficiency characteristics. The transmission of the two hybrid systems is different, especially the gear connected to the engine. However, for the DMI-AWD and the distributed drive mode of the MMC-AWD, the transmission ratios from the engine or the motor to the wheels are all the same.

5.3 Model Accuracy Verification

The foundation of economy analysis is a good vehicle's dynamic response. The SOC changes are validated in the following simulation.

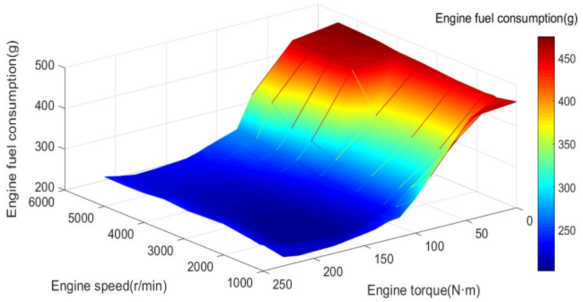

Figure 8 Engine fuel consumption

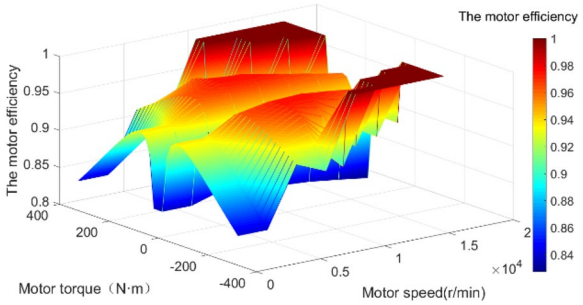

Figure 9 Front motor efficiency

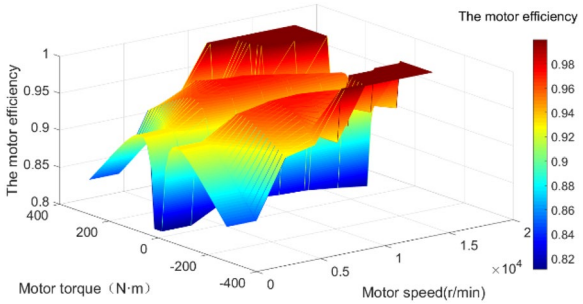

Figure 10 Rear motor efficiency

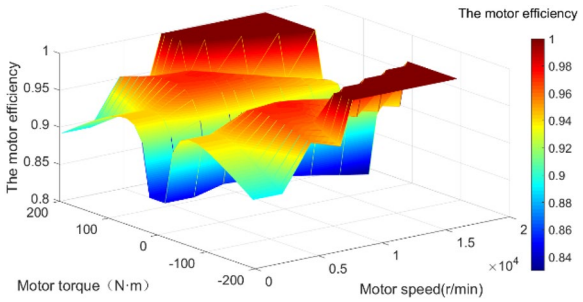

Figure 11 Generator efficiency

The high vehicle load, high energy consumption, and more obvious power demand of world light vehicle test procedure (WLTP) are due to the rapid changes in vehicle

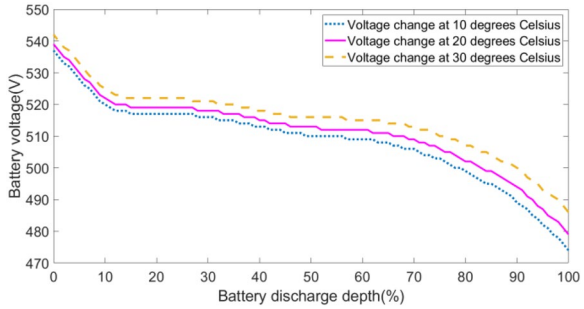

Figure 12 Diagram of discharge depth and voltage

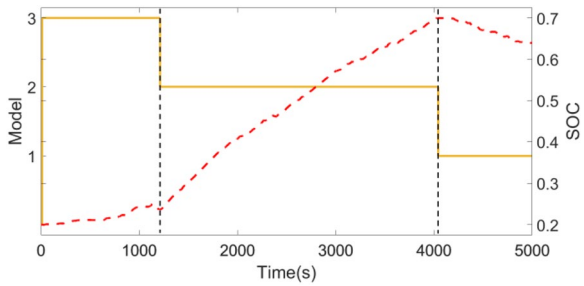

Figure 13 The mode corresponds with SOC

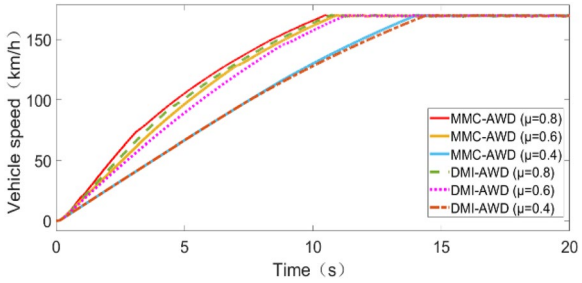

Figure 14 100 km/h acceleration time comparison chart

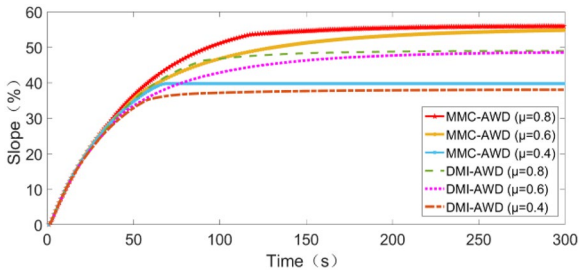

Figure 15 Comparison chart of maximum climbing degree

speed. The next step is to confirm the SOC changes under WLTP conditions when the vehicle starts with various SOC initial values and to evaluate the strategy's accuracy. As shown in Figure 13, in the case of a power shortage, the control strategies are transformed from 3 to 1. The battery power goes through three stages: slow replenishment, fast replenishment, and consumption.

The simulation results demonstrate that the first strategy consumes power gradually, the second strategy maintains a quick power replenishment speed when driving in series for an extended period of time, and the third strategy continues to meet the charging demand when the engine is the only source of driving power. The control strategy can accommodate cyclical conditions because the model is more precise.

5.4 Vehicle Power Performance Analysis

The simulation results in Figure 14 show that under the adhesion conditions of 0.8 and 0.6, the acceleration of 100 km/h is improved by 5.26% and 7.92%, respectively. It can be observed that the acceleration performance of the MMC-AWD system improves the most under moderate road adhesion conditions.

Create a slope with a variable gradient. Figure 15 illustrates the highest gradient the car may ascend while traveling slowly. According to the simulation results, the maximum gradeability rises on the high-adhesion, medium-adhesion, and low-adhesion roads of 0.8, 0.6, and 0.4, respectively, by 14.22%, 12.88%, and 4.55%.

On high adhesion surfaces, the MMC-AWD system's maximum climbing degree is significantly improved. The lower the adhesion coefficient, the lower the slope that can be climbed, but even with the lowest adhesion coefficient, the maximum climbing degree is still improved.

5.5 Vehicle Economy Analysis

5.5.1 MPC Controller Simulation Results

The analysis of the economic simulation is performed following the examination of power performance. Utilizing new European driving cycle (NEDC) conditions, respectively, yields the torque change and MPC controller output. Figures 16 and 17 show the simulation results.

To maintain the overall road torque demand, engine and motor torques are switched. While a negative motor torque shows the recovery of braking energy, a positive motor torque implies drive. As seen in Figure 17, the engine takes over the position of the motor when the load is heavy. However, the engine doesn't always start with a heavy load. Whether or not it starts is determined by the MPC computation of the motor efficiency, engine fuel consumption, and other parameters.

The MPC controller begins to compute energy consumption, indicating that the vehicle speed and road load have reached the fundamental requirements for engine ignition. When the engine's fuel consumption is less than the motor's equivalent fuel consumption,

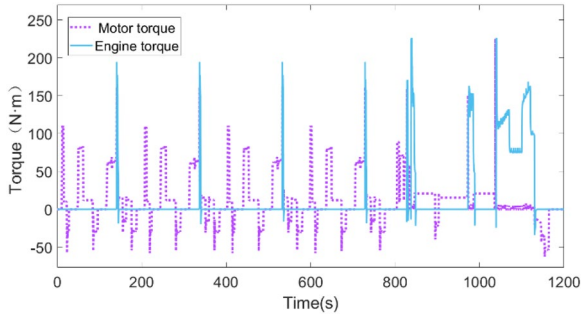

Figure 16 Engine and motor torque variation diagram for the NEDC condition

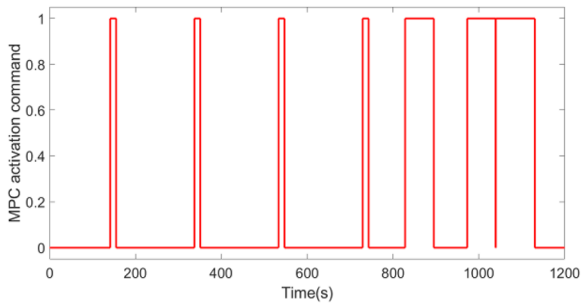

Figure 17 Controller activation time under NEDC condition

the engine operates in place of an electric motor; otherwise, the engine shuts off and the motor activates. The car can attain maximum energy efficiency in this situation.

5.5.2 Economy Comparison of Power Shortages and Short Working Cycles

Both systems were simulated using NEDC conditions. Three duty cycles, each with a duty time of 1200 s, are used in the simulation that follows. Due to the battery's low capacity, the car uses more fuel and increases its battery power from 40% to 70% during the first 1800 s. The economies of the MMC-AWD and DMI-AWD are compared when the battery is in the low state, and the results are shown in Figures 18 and 19.

When compared to the MMC-AWD's equivalent fuel consumption, the MMC-AWD consumes less SOC but more fuel, which still improves the economy. SOC is initially set at 40%. If the battery power is increased, it is calculated as the recovered fuel consumption, which is subtracted from the total fuel consumption. If the power decreases, it is converted into additional fuel consumption, and added to the total fuel consumption to get the final equivalent fuel consumption.

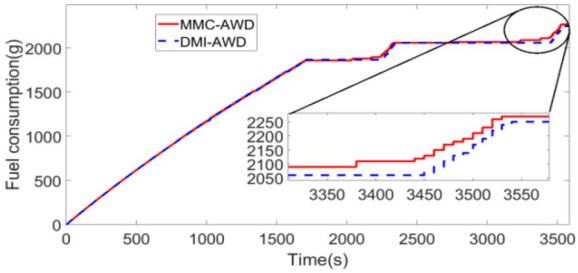

Figure 18 Diagram of fuel consumption under short-term working conditions with insufficient battery power

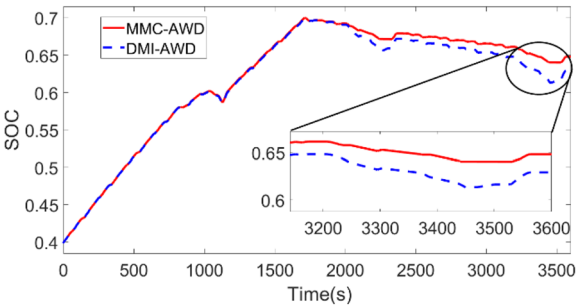

Figure 19 Diagram of SOC change chart of short-term working condition with insufficient battery power

5.5.3 Economy Comparison of Power Shortages and Long Working Conditions

The simulation uses NEDC conditions. When the battery is low, the engine must be used. The DMI-AWD uses parallel drive to adjust the output torque of the motor to maintain the engine's optimal operating point while starting the engine when there is a high demand for torque and low battery power. When the battery power is low and the torque demand is low, the engine in the MMC-AWD operates in series drive. When the torque demand is high, the engine operates in direct drive. Both the engine and the motor start and operate in parallel to move the vehicle under extremely high torque. The results for fuel and electricity consumption are displayed in Figures 20 and 21. Twelve cycles under the scenario of insufficient power were simulated in order to reflect the energy loss during charging and discharging.

In terms of economics, the rear motor's ability to maintain high efficiency at low torque is advantageous. Rear motor drive is preferred by both systems. Electricity is produced by both the generator of the DMI-AWD and the front motor of the MMC-AWD. When under heavy loads, the engine operates in parallel or direct drive.

Figures 22 and 23 are two diagrams that show the operating points of the motor and engine. As can be observed, the motor of the DMI-AWD system frequently recovers energy and compensates torque at low torque to maintain

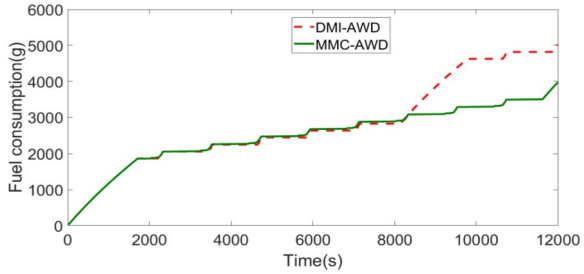

Figure 20 Fuel consumption diagram of long-term working condition with insufficient battery power

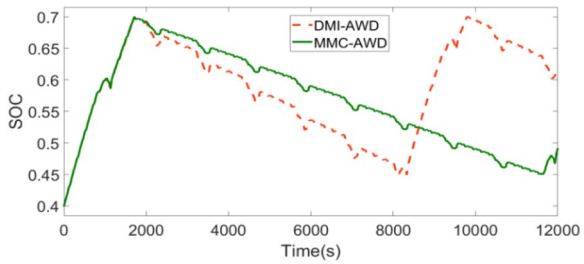

Figure 21 SOC variation diagram of long-term working condition with insufficient battery power

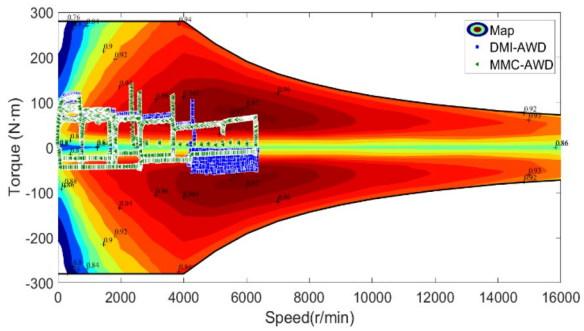

Figure 22 Motor operating points Comparison

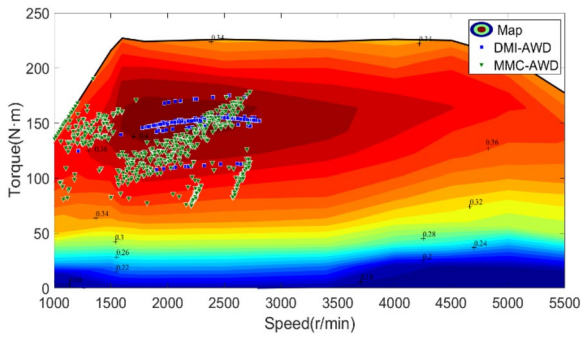

Figure 23 Engine operating points Comparison

the engine's maximum energy efficiency. However, motor efficiency is currently not very high. The operating point under low torque does not need to be adjusted by the motor when the engine is more efficient. The power source can achieve its highest overall efficiency at this point.

Table 4 provides an overview of the fuel usage and SOC changes. It is possible to determine the equivalent fuel usage and compare the two systems economically. Table 4 also includes equivalent fuel consumption information.

From the calculations in Table 4, it can be seen that the equivalent 100 km of fuel consumption can be reduced by 5% under the short-range condition. The equivalent of 100 km of fuel can be saved by 12.06% when the battery power is insufficient and in long-range condition. And the engine needs to charge the battery for a long distance. The MMC-AWD is economically sound.

The control method proposed in this paper obtains the best transient results in the predicted time domain. The method lies in inputting the fuel consumption equations and the power consumption equations into the MPC controller for calculation. However, the controller's settings must be adjusted, the set of equations must be revised, and the equivalent fuel consumption equation altered if additional power sources are added or the drive path is altered. This area of research will be studied as a next step.

6 Conclusions

(1) To achieve vectored distribution and full system power utilization between the axles, as well as to actualize centralized and distributed driving of the rear and front axles, the MMC-AWD is proposed for hybrid vehicles. Eight two-wheel drive, sixteen four-wheel drive, and brake energy recovery modes are available. The system has a very high overall performance.

(2) In order to accurately identify the driving force and braking force needed by the road surface and to achieve a good speed following effect in the two test conditions, a nonlinear driving force observer is established. Three distinct control strategies are established to switch among nine modes to replenish power under any SOC and high load conditions. A control strategy selection system based on SOC changes is created.

(3) The MPC minimum energy consumption controller based on the equivalent fuel coefficient is created. The average power and fuel consumption are then calculated in the MPC prediction time domain in order to switch the power source and achieve the lowest possible instantaneous equivalent fuel con-

Table 4 Equivalent fuel consumption calculation

Different system	Working condition	Fuel consumption (g)	Changes of SOC (%)	Equivalent fuel consumption (L/100 km)
DMI-AWD	Short working cycle	2252.4	40–62.92	5.39
	Long working condition	5008	40–61.74	5.14
MMC-AWD	Short working cycle	2268.3	40–64.80	5.12
	Long working condition	3957	40–49.17	4.52

sumption. When the axle load is transmitted, the MMC-AWD transmission is utilized to actualize the concentrated front axle drive and distributed rear axle drive and transfer the front axle's power to the rear axle, improving dynamic performance.

(4) The same power source and fundamental vehicle parameters are used to create a comparative model. It has been demonstrated that a road with an adhesion coefficient of 0.8 and 0.6 increases acceleration at 100 km/h by 5.26% and 7.92%, respectively. A road with an adhesion coefficient of 0.8, 0.6, and 0.4 increases maximum grade ability by 14.22%, 12.88%, and 4.55%, respectively. According to the simulation results, the MMC-AWD still outperforms the DMI-AWD in terms of economy under long-range operating conditions with insufficient battery power. There is a 12.06% reduction in fuel consumption from 5.14 L of crude oil to 4.52 L.

Abbreviations

N_2	Engine clutch command
SOC	Battery state of charging
SOC_L	Lower limit of SOC
SOC_C	Charging point of SOC
SOC_H	Upper limit of SOC
T	Vehicle driving torque demand
T_{eff}	Lower limit of engine-efficient torque
T_{ecmd}	Engine torque command
T_{emax}	Engine maximum torque
T_{mr}	Rear motor maximum torque
T_{mf}	Front motor maximum torque
T_{mcmd}	Motor torque command
K	Road adhesion coefficient
F_{xf}	Front axle adhesion force
F_{xr}	Rear axle adhesion force
i_{3_switch}	Charge switching instruction
T_{er}	Current engine torque
T_b	Braking torque
N_1	Generator controller activation instruction
T_m	Motor driving torque
T_e	Engine output torque
T_{max}	Motor maximum torque with current speed
V_{ne}	Actual engine speed
i	Clutch transmission ratio
η	Clutch transmission efficient
i_1	Centralized transmission ratio
η_1	Centralized transmission efficient
i_2	Distributed transmission ratio
η_2	Distributed transmission efficient
n_e	Actual engine speed
n_{e0}	Engine ignition speed
n_{e1}	Low limit of engine-efficiency speed
n	Generator command
T_L	Low-grade torque
T_M	Medium-grade torque
T_H	High-grade torque
d_{Vi}	Speed difference between actual and command value

Acknowledgements
Not applicable.

Authors' Contributions
LZ was in charge of the whole trial; ZW wrote the manuscript; LW and CR assisted with sampling and laboratory analyses. All authors read and approved the final manuscript.

Funding
Supported by Hebei Provincial Natural Science Foundation of China (Grant Nos. E2020203174, E2020203078), S&T Program of Hebei Province of China (Grant No. 226Z2202G), and Science Research Project of Hebei Provincial Education Department of China (Grant No. ZD2022029).

Data availability
The authors confirm that the data supporting the findings of this study are all results of bench tests and model simulations, which available within the article.

Declarations

Competing Interests
The authors declare no competing financial interests.

Received: 11 July 2022 Revised: 11 January 2024 Accepted: 23 February 2024
Published online: 25 March 2024

References

[1] B Lin, L Shi. Do environmental quality and policy changes affect the evolution of consumers' intentions to buy new energy vehicles. *Applied Energy*, 2022, 310: 118582.
[2] G J Offer, D Howey, M Contestabile, et al. Comparative analysis of battery electric, hydrogen fuel cell and hybrid vehicles in a future sustainable road transport system. *Energy Policy*, 2010, 38(1): 24-29.
[3] C Silva, M Ross, T Farias. Evaluation of energy consumption, emissions and cost of plug-in hybrid vehicles. *Energy Conversion & Management*, 2009, 50(7): 1635–1643.
[4] X Tang, Z Duan, X Hu, et al. Improving ride comfort and fuel economy of connected hybrid electric vehicles based on traffic signals and real road information. *IEEE Transactions on Vehicular Technology*, 2021, 70(4): 3101–3112.
[5] D F Opila, X Wang, R Mcgee, et al. An energy management controller to optimally trade off fuel economy and drivability for hybrid Vehicles. *IEEE Transactions on Control Systems Technology*, 2012, 20(6): 1490–1505.

[6] Y He, K H Kwak, Y Kim, et al. Real−time torque−split strategy for P0+P4 mild hybrid vehicles with eAWD capability. *IEEE Transactions on Transportation Electrification*, 2022, 8(1): 1401− 1413.
[7] L Zhang, W Liu, B Qi. Innovation design and optimization management of a new drive system for plug-in hybrid electric vehicles. *Energy*, 2019, 186: 115823.
[8] T Park, H Lee. Optimal supervisory control strategy for a transmission−mounted electric drive hybrid electric vehicle. *International Journal of Automotive Technology*, 2019, 20(4): 663−677.
[9] M Ye, D Qin, Z Liu. Research on dynamic shift law of mild hybrid AMT vehicle. *Automotive Engineering*, 2006(7): 671−675.
[10] H Guo, Q Sun, C Wang, et al. A systematic design and optimization method of transmission system and power management for a plug-in hybrid electric vehicle. *Energy*, 2018, 148: 1006−1017.
[11] J Cho, K Huh. Torque vectoring system design for hybrid electric–all wheel drive vehicle. *Proceedings of the Institution of Mechanical Engineers, Part D: Journal of Automobile Engineering*, 2020, 234(10−11): 2680−2692.
[12] F Ju, W Zhuang, L Wang, et al. Comparison of four-wheel-drive hybrid powertrain configurations. *Energy*, 2020, 289: 118286.
[13] F Ju, W Zhuang, L Wang, et al. The optimal sizing and the adaptive energy management of a will be four-wheel-drive hybrid powertrain. *Energy*, 2019, 187: 116008.
[14] A Goodarzi, M Mohammadi. Stability enhancement and fuel economy of the 4-wheel−drive hybrid electric vehicles by optimal tyre force distribution. *Vehicle System Dynamics*, 2014, 52(4): 539− 561.
[15] C Wu, J Ruan, H Cui, et al. The application of machine learning based energy management strategy in multi-mode plug-in hybrid electric vehicle, part I: Twin delayed deep deterministic policy gradient algorithm design for hybrid mode. *Energy*, 2023, 262: 125084.
[16] Y Ma, C Li, S Wang. Multi−objective energy management strategy for fuel cell hybrid electric vehicle based on stochastic model predictive control. *ISA Transactions*, 2022, 131: 178−196.
[17] D Wang, M Hu, B Li, et al. Modular modeling and dynamic response analysis of a driveline system during start−up process. *Mechanism and Machine Theory*, 2021, 156: 104136.
[18] Z Liu, S Cheng, J Liu, et al. A novel braking control strategy for hybrid electric buses based on vehicle mass and road slope estimation. *Chinese Journal of Mechanical Engineering*, 2022, 35: 150.
[19] J Liao, Y Yang, H Luo, et al. Energy management strategy of four-wheel drive SUV electric-hydraulic hybrid (EHH) power system based on optimal instantaneous efficiency. *Sustainable Energy Technologies and Assessments*, 2022, 52: 102139.
[20] L Hu, Q Tian, C Zou, et al. A study on energy distribution strategy of electric vehicle hybrid energy storage system considering driving style based on real urban driving data. *Renewable and Sustainable Energy Reviews*, 2022, 162: 112416.
[21] F Wang, J Xia, Y Cai, et al. Novel energy management strategy for a dual−motor hybrid electric vehicle considering frequency of mode transitions. *Energy Conversion and Management*, 2022, 269: 116106.
[22] L Zhang, W Liu, B Qi. Energy optimization of multi−mode coupling drive plug-in hybrid electric vehicles based on speed prediction. *Energy*, 2020, 206: 118126.
[23] H Dong, W Zhang, G Yin, et al. Energy-optimal braking control using a double−layer scheme for trajectory planning and tracking of connected electric vehicles. *Chinese Journal of Mechanical Engineering*, 2021, 34: 83.
[24] B P Adedeji. A multivariable output neural network approach for simulation of plug-in hybrid electric vehicle fuel consumption. *Green Energy and Intelligent Transportation*. 2023, 2: 100070.
[25] Y J Liu, Q Sun, C Z Liu, et al. Fuel consumption optimization for a plug-in hybrid electric bus during the vehicle−following scenario. *Journal of Energy Storage*, 2023, 64: 107187.
[26] H Li, A Raveya, A N'Diaye, et al. A novel equivalent consumption minimization strategy for hybrid electric vehicle powered by fuel cell, battery and supercapacitor. *Journal of Power Sources*, 2018, 395: 262−270.
[27] R H Zhang, N Wu, Z H Wang, et al. Constrained hybrid optimal model predictive control for intelligent electric vehicle adaptive cruise using energy storage management strategy. *Journal of Energy Storage*, 2023, 65: 107−183.
[28] Y Z Wang, P J Jin. Model predictive control policy design, solutions, and stability analysis for longitudinal vehicle control considering shockwave damping. *Transportation Research Part C*, 2023, 148: 104038.
[29] L Guo, L Hui, L Han, et al. Predictive energy management strategy of dual−mode hybrid electric vehicles combining dynamic coordination control and simultaneous power distribution. *Energy*, 2023, 263: 125598.
[30] T Liu, X Zeng, D F Song. MPC-based coordinated control of gear shifting process for a power-split hybrid electric bus with a clutchless AMT. *Chinese Journal of Mechanical Engineering*, 2022, 35: 144.

Lipeng Zhang born in 1979, is currently a professor at *Yanshan University, China.* He received his PhD degree from *Beijing Institute of Technology, China,* in 2011. His research interests include intelligent vehicle dynamics and control, new energy vehicle compound transmission, driver awareness, and driving assistance.

Zijian Wang born in 1997, is currently a master candidate at *Hebei Key Laboratory of Special Delivery Equipment, Yanshan University, China*.

Liandong Wang born in 1967, since 2001, he has been a professor at *Department of Automotive Engineering, School of Vehicle and Energy, Yanshan University, China.* His research interests are passenger car and commercial vehicle parts development and application.

Changan Ren born in 1994, is currently a PhD candidate at *Hebei Key Laboratory of Special Delivery Equipment, Yanshan University, China.*